

CHARACTERIZATION OF THE DAMAGE BEHAVIOR OF RECYCLED CARBON FIBER WITH X-RAY AND ACOUSTIC EMISSION TECHNIQUES

Christian Becker^{1*}, Nicole Motsch-Eichmann¹, Joachim Hausmann¹

¹: Leibniz-Institut für Verbundwerkstoffe GmbH, Kaiserslautern, Germany

*corresponding author: christian.becker@ivw.uni-kl.de

Keywords: Recycled carbon fibers, In-situ measurement, X-Ray microscopy, mechanical properties, sizing

ABSTRACT

This article deals with the characterization of the damage behavior of recycled carbon fiber (rCF) roving's that are further processed into unidirectional (UD) reinforced plastic panels. In the first step, the mechanical properties of different material combinations are determined by mechanical tests (tension, bending). This proves the usability of this material for load-bearing constructions. Subsequently, the fracture surface is analyzed by scanning electron microscopy (SEM) to characterize the fiber-matrix adhesion and to obtain first indications of possible failure mechanisms. Smaller samples are tested in pre-determined load levels in transverse tensile and bending tests. The 3-dimensional scan reconstruction results are used to visualize the failure behavior of the staple fibers in order to detect fiber pull-out, fiber or inter-fiber failure and to draw initial conclusions on the damage behavior compared to classic fiber composites. In combination with the SEM images and the mechanical parameters, these results can provide initial conclusions on the failure behavior of components made of rCF staple fiber yarn. Furthermore, first concepts and experiments for the integration of the AE analysis into the in-situ setup of the X-ray microscope are shown.

1 INTRODUCTION

The use of fiber-reinforced components for lightweight constructions is rapidly increasing over the past decade. The rising amount of waste per year leads to an increasing requirement to develop new techniques for recycling and reuse of carbon fiber [1]. To fulfill environmental and economic goals, upcycling of end-of-life products and production waste into structural components must be achieved. Several techniques have been developed to extract the fibers out of the matrix. The separation of fibers can be done chemically (solvolysis) or thermally (pyrolysis). The pyrolysis is actually the most commonly used process [2]. All processes lead to a loss of fiber length because of cutting the components to smaller parts, which can be handled during the treatment [3]. The fiber length is reduced differently through these processes and new pre-products have to be made out of this shorten fibers (non-woven, woven or staple fiber yarn (roving's)) [4, 5]. One product, which is commercially available, is a rCF-roving from the Wagenfelder Spinnerei GmbH (Germany). This product stands out due to the fixation through a binding yarn.

In this work, the mechanical behavior of unidirectional (UD) reinforced plates out of recycled carbon fiber (rCF)-rovings is investigated. Previous research showed a good mechanical performance of this material although a poor fiber-matrix attachment was detected [6]. By means of mechanical tests with different matrix systems, the influence of the missing sizing on the mechanical properties of rCF-plates is investigated. These are determined by static tensile, compressive and bending tests. In these tests acoustic emission (AE) analysis is integrated to detect damage events. Afterwards the fracture surface is analyzed by scanning electron microscopy (SEM) to characterize the fiber matrix adhesion and get first indications of possible failure mechanisms. Smaller samples will be tested under predefined load levels and the failure behavior is investigated in-situ using X-Ray microscopy. With this, the failure behavior of the staple fibers is visualized in order to detect fiber pull out, fiber- or inter-fiber failure and to draw first conclusions about the damage behavior in comparison to classic fiber composites. Additionally there will be tests integrating the acoustic emission analysis into the in-situ device.

2 METHODOLOGY

Previous work with unidirectional reinforced plates of rCF staple fiber yarn (rCFRP plates with 40 % fiber volume content) with a bio-based matrix system has shown good mechanical properties with a Young's modulus of 80 GPa and 700 MPa tensile strength. [6] However, scanning electron microscopy studies of the fracture surfaces showed almost no fiber-matrix adhesion. This was mainly characterized by fiber pull-out behavior and interphase delamination. The reason for this is probably the pretreatment and history of the rCF fibers used in the staple fiber yarn (unfortunately, no manufacturer's information on this is available). Since the fibers are presumably from production residues that were reconditioned in the pyrolysis process and later processed into staple fiber yarns, the condition and type of sizing is unknown. This condition means that the use of different matrix systems can lead to varying degrees of fiber-matrix bonding. In order to assess this effect qualitatively, rCF UD sheets were produced using two different matrix systems (epoxy resin Huntsman Araldite® LY 1135-1 and PA6 film from own production) in a winding process adapted for the respective resin system (Figure 1). The EP resin was produced in a wet winding process with subsequent curing in an autoclave, whereas the PA6 film was placed between the dry wound rCF fibers in a film stacking process. This sheet was then impregnated and cured also in the autoclave. Since the optimal process parameters were not known, both processes resulted in lower values with 30 % fiber volume fraction than in the plates with 40 % fiber volume fraction used in [6]. Nevertheless, a comparison of the mechanical behavior can be made.

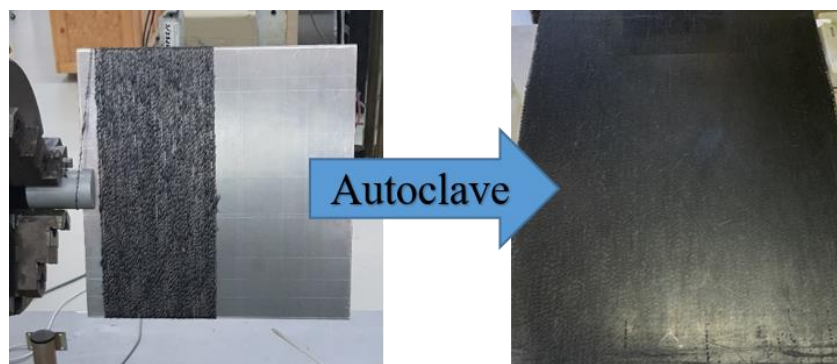


Figure 1: Plate winding process and final unidirectional rCF plates after autoclave cycle

Before the plates were wound, first scanning electromicroscopic images of the untreated rCF staple fibres were taken (Figure 2). Here it can be seen that there is no pure smooth carbon fiber but a light film on the fibre. This could be remnants from the original fibre sizing that were not completely dissolved in the pyrolysis process. In some cases, coarser particle adhesions can also be seen, which can also lead to a reduced adhesion of the new matrix to the fibres.

FTIR (Fourier Transform Infrared Spectroscopy) measurements are carried out to gain a more precise insight into which adhesions or sizing residues are present on the fiber. For this purpose, the rCF fibers were soaked in acetone for 24 hours to dissolve the sizing. By filtering and evaporating the solution, it could be separated and subsequently characterized. The results can be seen in Figure 3. The upper curve shows the analysis (interferogram) of the unknown sizing. The lower two curves show the two highest matches to the database (Table Figure 3).

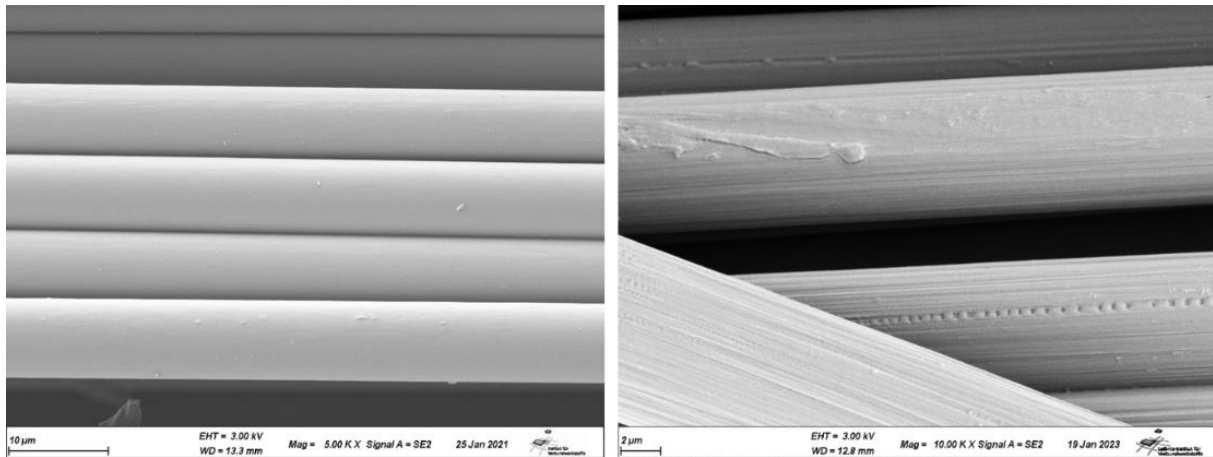
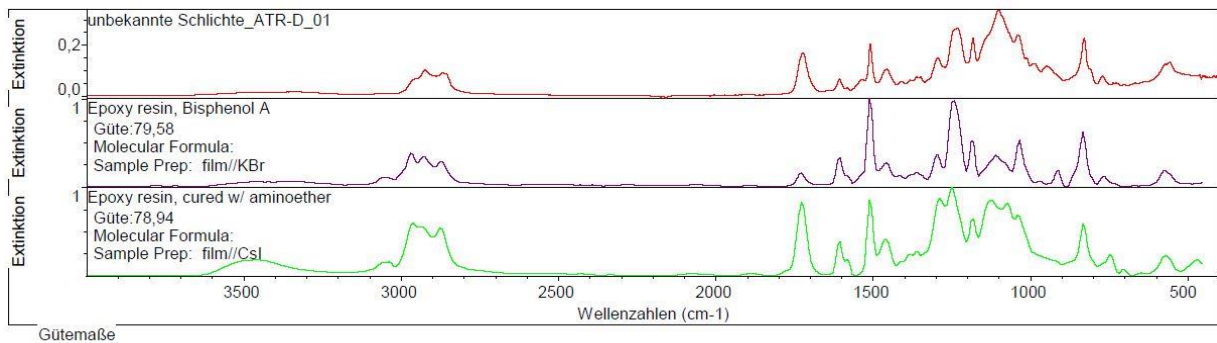


Figure 2: SEM images of the dry rCF fibers of the same charge with no visible adhesions (left) and visible unknown grooves plus film (right)



Index	Güte	Spektrename	Bibliothekname
1	179	79,58 Epoxy resin, Bisphenol A	Hummel Polymer and Additives
2	201	78,94 Epoxy resin, cured w/ aminoether	Hummel Polymer and Additives
3	200	78,45 Epoxy resin, cured w/ amidoamine	Hummel Polymer and Additives
4	199	78,21 Epoxy resin ester, Bisphenol A	Hummel Polymer and Additives
5	779	78,20 Epoxy resin mixture	HR Nicolet Sampler Library
6	479	77,66 EPOXY RESIN #4	HR Polymer Additives and Plasticizers
7	481	77,10 EPOXY RESIN #6	HR Polymer Additives and Plasticizers
8	725	77,10 Diglycidyl ether of bisphenol A mixture	HR Nicolet Sampler Library
9	480	77,02 EPOXY RESIN #5	HR Polymer Additives and Plasticizers
10	333	77,00 EPOXY RESIN #1	HR Polymer Additives and Plasticizers

Figure 3: FTIR analysis of sizing on rCF fibers.

The analysis gives an 80 percent match with a bisphenol A-based epoxy system. The exact sizing cannot be determined by the analysis, but a better suitability for epoxy resin systems can be assumed. In addition, it can be surmised that the rCF fibers used are from production residues and not from pyrolysis.

In general, the focus of this work is to investigate and describe the mechanical behavior of unidirectional rCF reinforced plastic under static load. For this purpose, tensile tests (following EN ISO 527-5), compression tests (following EN ISO 14126) and bending tests (following EN ISO 14125) are carried out in the first step. The characteristic values give a first impression whether differences due to the matrix system are recognizable. The general influence of the matrix should be negligible in UD tests in fiber direction with ideal fiber-matrix adhesion. Subsequently, the fracture surfaces of the tensile and flexural specimens are examined again in the SEM and the failure behavior is determined.

In order to gain a deeper insight into the failure mechanisms and to determine fiber/interfiber fractures and fiber pull-out behavior, in-situ tensile and bending tests are carried out in the X-ray microscope. The tests for this can currently only be carried out transverse to the fiber orientation. This

is mainly due to the sample geometry. By measuring in fiber direction the samples currently fails due to excessive stresses in the clamping and not within the gauge length. Thus, the tests are invalid according to the standard but cannot be evaluated in X-ray microscopy. First tests and approaches with a new geometry are explained in chapter 3.3. In this chapter also the acoustic emission tests and the concept of the unification of both methods is shown there.

3 RESULTS

In this chapter, the results of the individual tests are presented. First, the quasi-static mechanical tests are analyzed and the samples are examined microscopically (chapter 3.2). Subsequently, the in-situ tests in the X-ray microscope are discussed and the determined failure behavior is evaluated. Chapter 3.4 deals with the approach to integrate Acoustic Emission (AE) measurement techniques into in-situ X-ray microscopy. The new sample geometry is also considered here.

3.1 Mechanical Tests and microscopic characterization

As mentioned above, the mechanical tests were carried out in accordance with the standards EN ISO 527-5 (tension), EN ISO 14126 (compression) and EN ISO 14125 (bending) for the two matrix systems.

The results of the tensile tests are shown in the Figure 4 and Table 1. It can be seen that at the same elongation at break, the EP specimens with a modulus of elasticity of approx. 50,000 MPa and a strength of 550 MPa have about 10 % higher characteristic values than the PA6 specimens. The fracture patterns of the specimens are also similar, whereby the PA6 specimens break completely less frequently and the fracture surfaces are bridged by fiber strands (see Figure 4).

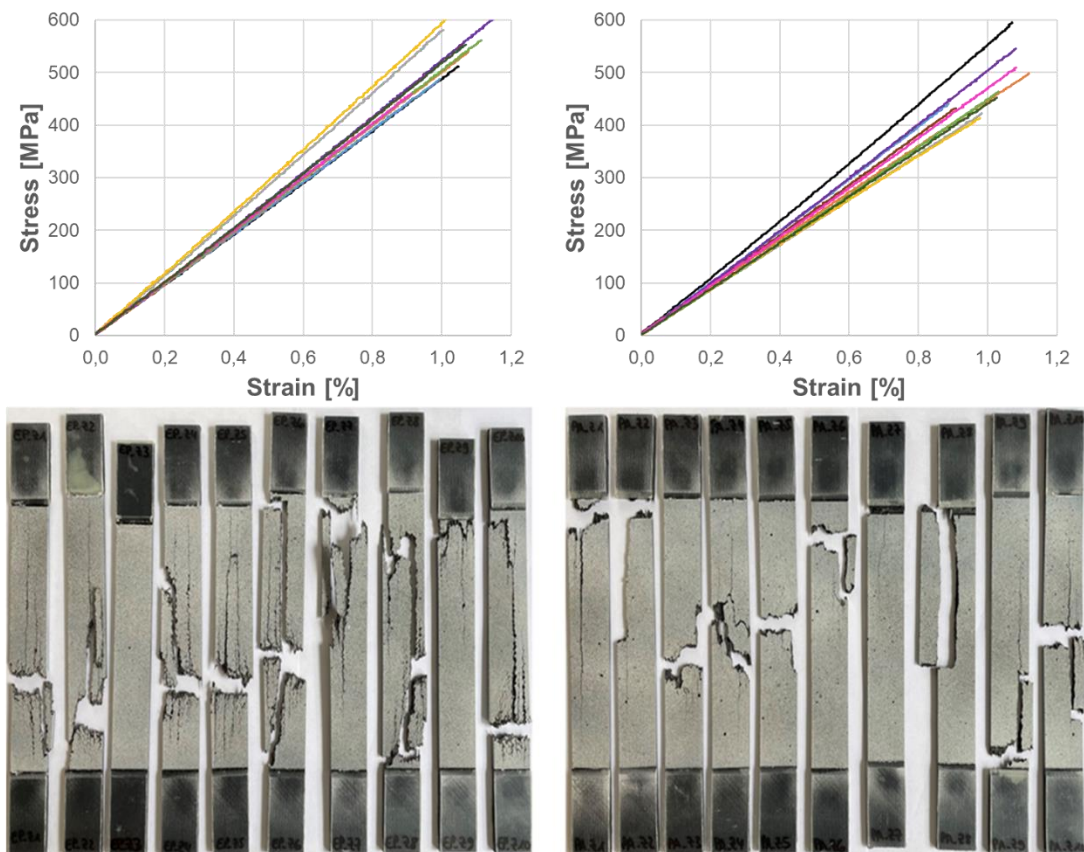


Figure 4: Stress-strain diagrams and correspondent failed samples of EP-rCF (left) and PA6-rCF (right)

Table 1: Mechanical properties of the rCF samples with Epoxy and PA 6 resin with percentage deviation <G> from each other

Matrix	Young's modulus (MPa)	Elongation (%)	Strength (MPa)
Epoxy	50271.47	1,05	551.31
PA 6	45849.74	1,04	488.10
<G>	<8.80>		<11.47>

However, looking at the SEM images of the fracture surfaces, it can be seen that the fiber-matrix adhesion between rCF fiber and the PA6 matrix has better properties than to the EP matrix. In Figure 5, it can be seen that fiber pull-out forms channels in both matrix systems. This indicates a less than optimal adhesion for both. However, in comparison, it can be seen in the left picture that clearly larger fiber pieces are free, on which no matrix residues can be seen. This speaks for a pure fiber pull-out behavior. In the right picture, on the other hand, clearly shorter fiber ends protrude from the material, which still show matrix residues in some places. The visible fiber channels could be signs of fiber breaks where the end was pulled out of the matrix. However, as with the EP samples, this could also indicate pure fiber extraction. This must be proven by further investigations.

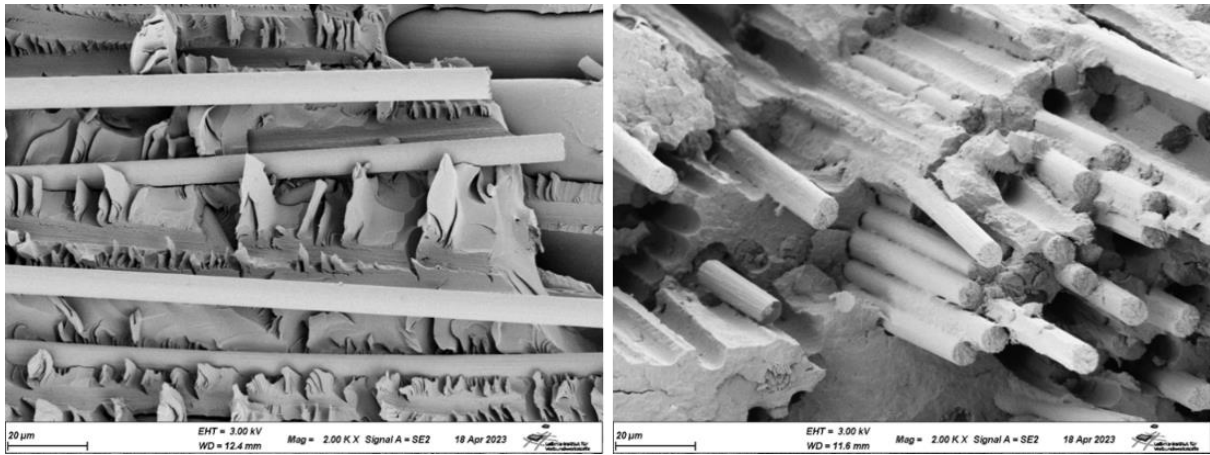


Figure 5: SEM images of fracture surface of EP-rCF (left) and PA6-rCF (right)

In general, however, the connection in both matrix systems is not ideal and one must rather speak of a poor fiber-matrix adhesion. It is interesting to note, however, that despite the better suitability of the existing sizing with epoxy resin systems found in the FTIR analysis, the SEM images tend to indicate that the PA6 system has better adhesion. However, the mechanical properties rather indicate that the EP resin system performs slightly better. Since both systems show the same elongation at break, aging processes in the PA6 due to longer storage time of the film or too high curing temperatures in the autoclave could be the reason for this effect.

The results of the bending test are shown in Figure 6 and Table 2

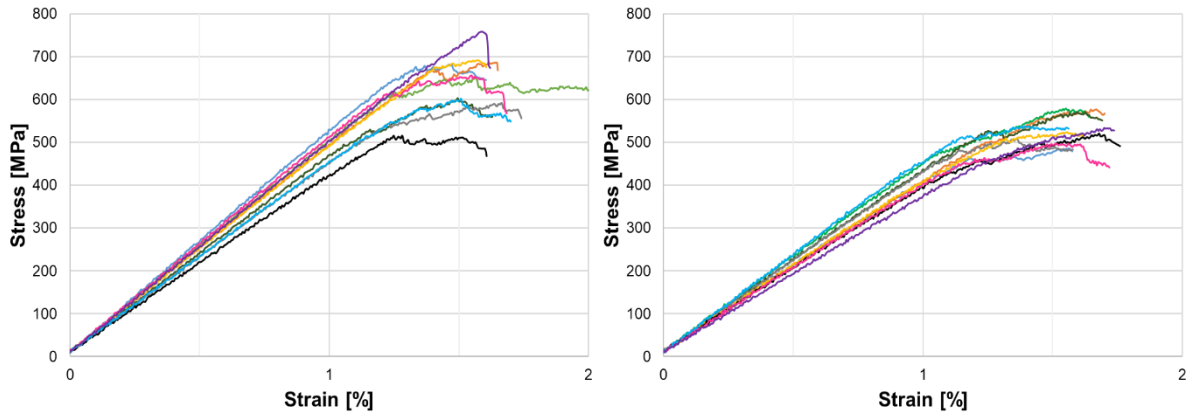


Figure 6: Stress-strain diagrams of the bending tests for EP-rCF (left) and PA6-rCF (right)

Table 2: Comparison of bending properties of both matrix systems with percentage deviation <G> from each other

Matrix	Bending Modulus [MPa]	Strain [%]	Bending strength [MPa]
Epoxy	48212.77	1,69	597.65
PA 6	41266.07	1,66	515.00
<G>	<14.41>		<13.83>

Here, too, the picture is similar to that of the tensile tests. The EP specimens have a higher strength and a higher bending stiffness at a similar elongation. The fracture pattern looks similar for both variants. No delaminations are visible, but mainly failure in compression (top side) and tension (bottom side) and the associated crack growth under 45° through the specimen.

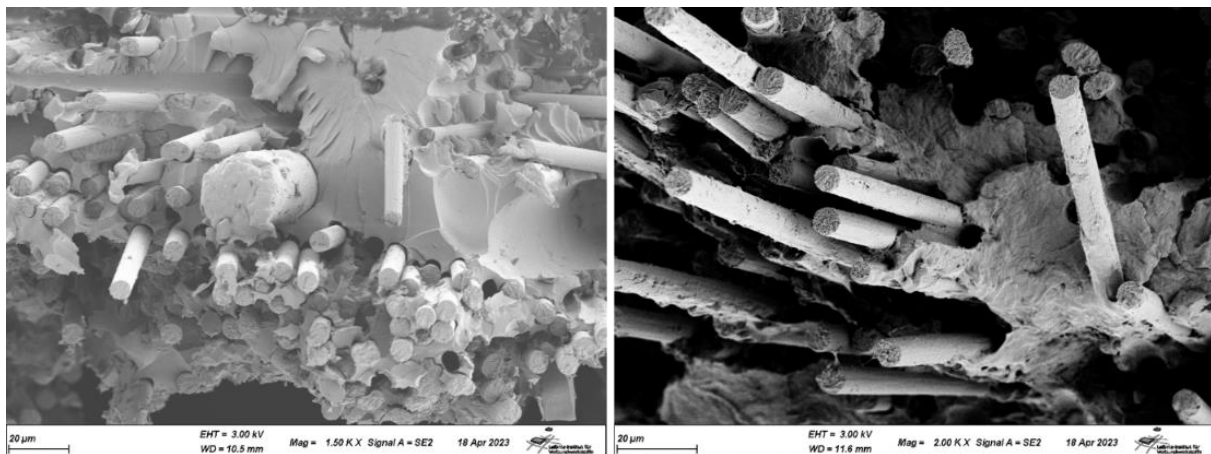


Figure 7: SEM images of the fracture surface of the EP (left) and PA6 (right) bending samples

If we now look at the SEM images of the fracture surfaces in Figure 7, we see nearly the same picture as for the tensile tests. Pull-out channels are visible in both. The EP sample on the left shows clear detachments between fiber and matrix, but hardly any matrix adhesion to the exposed fibers. In the PA6 samples on the right, however, clear matrix adhesions can be seen despite the presence of pull-out channels, which indicates better bonding behavior. Once again,

these findings do not reflect the mechanical properties, where the EP samples show approx. 16 % higher characteristic values than the PA 6 samples.

3.2 In-situ X-ray microscopy

The test set-up for the in-situ transverse tensile tests is shown in Figure 8 together with the specimen geometry used. The test series were carried out as a load increase test. After reaching a defined load level, the tensile test was stopped, the specimen was relaxed (to avoid undesired movement artefacts in the CT scan) and then a 360° scan was performed. This was carried out until the specimen failed.

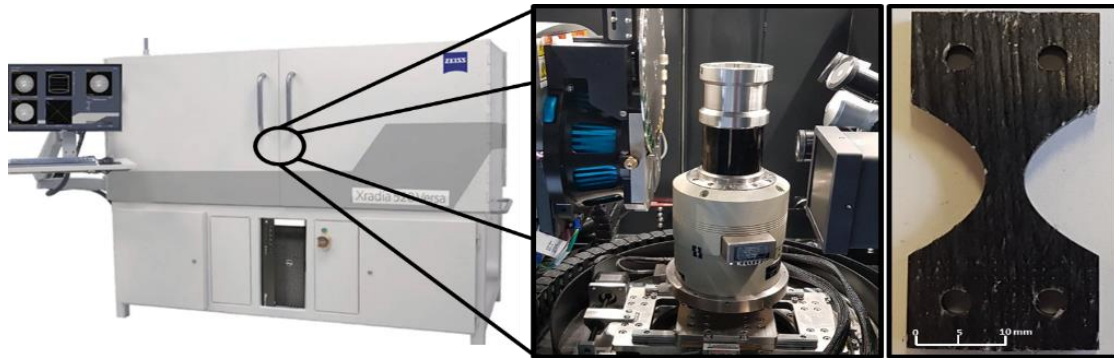


Figure 8 X-Ray Microscope Zeiss Xradia 520 Versa with in-situ module Deben CT 5000 and used sample geometry (right)

In order to get a first impression of the failure behavior of the specimens, preliminary tests were carried out to determine the load levels for the test. These are shown in Figure 9 on the left. Figure 9 on the right shows the force-displacement curve of the load increase test. It can be seen that the breaking force of 350 N is approx. 40 % higher than the mean value (around 250 N) of the preliminary tests (16 % higher than the maximum value (300 N)). This is due to relaxation effects in the material. Keeping the sample at a constant strain level for a long time causes the sample to relieve internal stresses. This leads to an increase in the maximum load that can be sustained. These effects lead to stronger alignment of fibers in the direction of the load, resulting in stiffening of the material. This is confirmed by the decrease in elongation at break from 0.3 mm on average to 0.25 mm.

A total of 9 load levels were measured, which are divided as follows after a relaxation time (adjust constant load):

1. 20 N pre-load
2. 70 N, relaxation to 65 N
3. 120 N; relaxation to 90 N
4. 170 N; relaxation to 145 N
5. 220 N; relaxation to 180 N
6. 250 N; relaxation to 230 N
7. 300 N; relaxation to 270 N
8. 350 N; failure
9. 20 N; crack opening

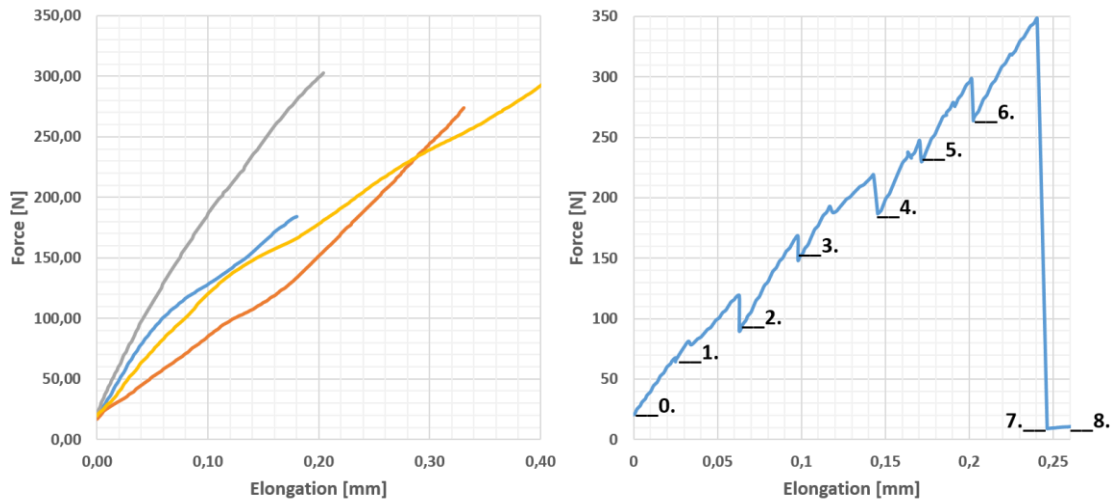


Figure 9: Force-elongation diagram from the pre-tests of the rCF-in situ samples EP-rCF normal to the fiber orientation. (left) and diagram during in-situ experiment with load levels; relaxation of sample visible (right)

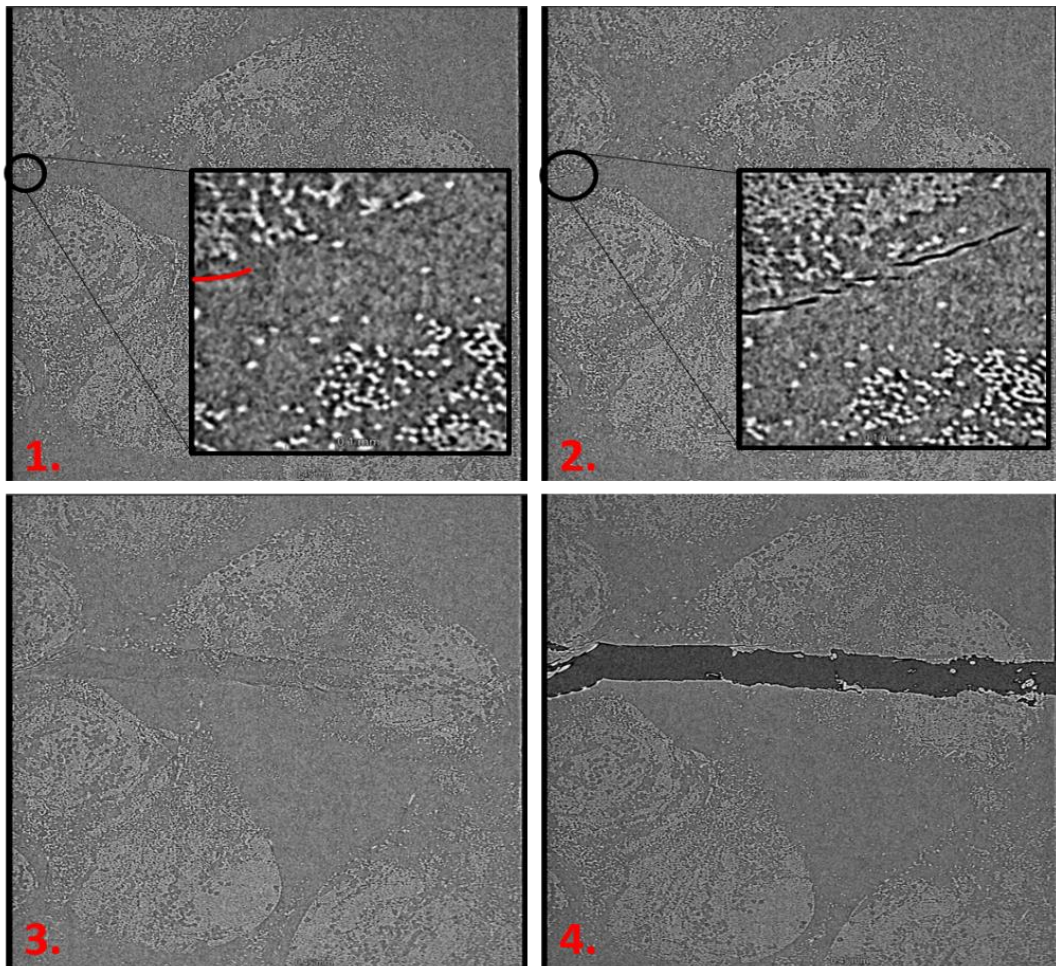


Figure 10: Volume rendering images of in situ tensile test of EP-rCF: 1) 250 N; small crack (red line) at the edge of sample. 2) 300 N: crack propagation between the fibers. 3) 350 N: failure of the sample. 4) Crack opening of 0.1 mm

Figure 10 shows exemplary sectional views of load levels 5 to 8, illustrating crack initiation, crack growth and post-failure.

In Figure 10. 1, a slight crack is visible (marked in red for better visualization). The crack initiation starts within a roving that is slightly above the narrowest part of the specimen (normally the maximum stress under tensile load is in the narrowest part of the tailored specimen). When the load is increased to 300 N, the crack continues to expand through the roving (Figure 10 2). In Figure 10 3 at 350 N, the complete failure of the specimen takes place. It can be seen that the crack that penetrates the entire specimen is not identical to the crack seen in the previous load levels. This suggests that micro-cracks are already present in the previous load levels, which were not visible in the CT scan, but lead to failure due to the stress maximum at the narrowest point. Figure 10 4 shows the post-failure, where the crack has widened by 0.1 mm. It can be seen that individual fiber strands bridge the crack and thus maintain the structural cohesion of the specimen ("fiber bridging"). No more load is applied to the specimen (constant load at 20 N) and only fiber pull-out from the interconnected fracture surfaces takes place. This behavior can also be verified by SEM images of the failed specimens from the quasi-static mechanical tests, where fiber bridging also occurred (cf. fiber channels visible).

3.3 Integration of acoustic emission in in-situ setup

In order to integrate the sensors of the AE apparatus into the Deben CT 5000 in-situ module, new clamps must first be developed that allow the sensors to be guided through the closed construction into the interior. The clamps were designed in such a way that a new sample geometry developed in [7] can be used. The structure including the specimen can be seen in Figure 11.

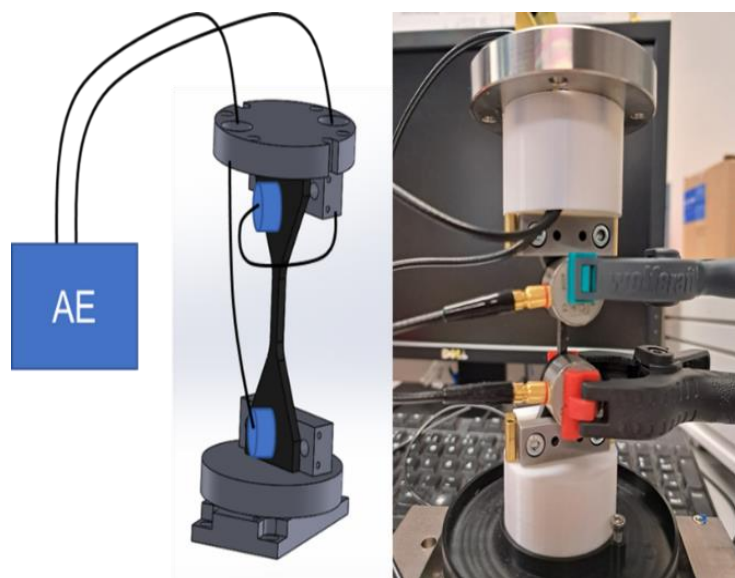


Figure 11: Integration of AE sensors into In-situ Deben CT 5000: Construction drawing (left) and final setup (right)

First AE tests (no in-situ tests) on the rCF test specimens showed that the general setup works. The sensor positioning is sufficient to get a large scan field of the sample. Also the sensor position delivers conclusive signals. The results of one Bio-rCF sample with the new test setup and sample geometry is shown in Figure 12.

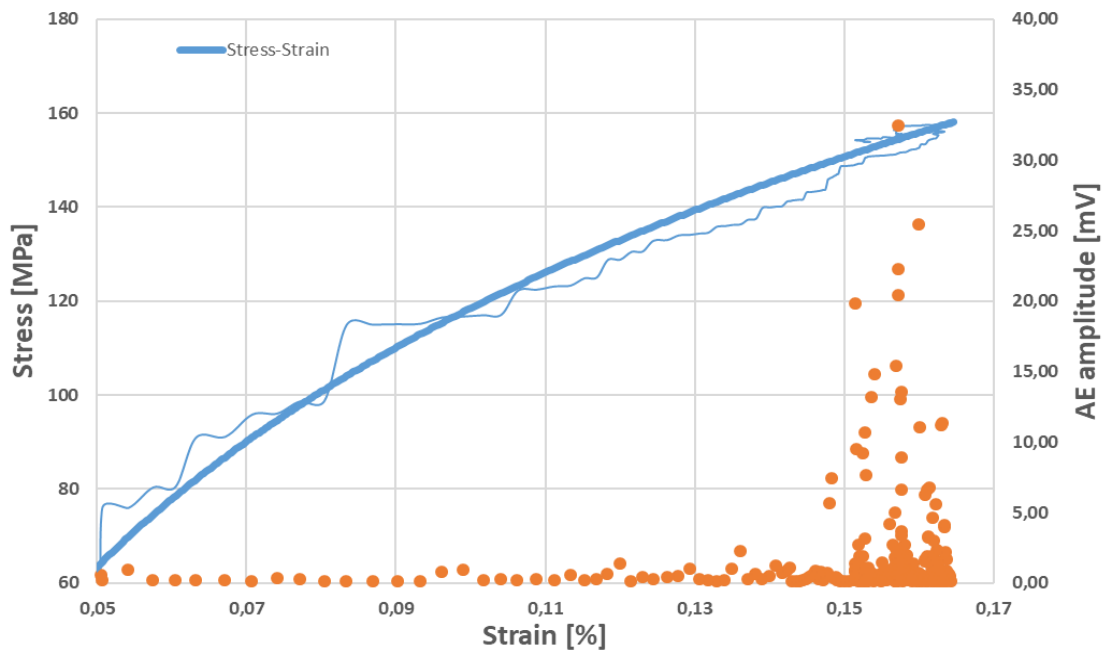


Figure 12: Example of stress-strain diagram of Bio- rCF sample with AE signal distribution

The typical stress-strain curve for the rCF material (blue line) is shown. The orange dots represent the recorded AE events, which provide clues to events in the material. Here it can be seen that up to an elongation of 0.13 % no conspicuous signals were recorded. From there on, not only does the number of recorded events increase (increase in point density), but there is also a clear increase in the amplitude of the signals, especially from 0.15 % strain. This increase correlates with the onset of damage and ultimately the failure of the specimen at 0.17 % strain in the tensile test. This in turn means that the acoustic signals have detected initial damage in the material.

In order to obtain more precise conclusions and interpretations about the AE signals of the rCF samples, more measurement series are planned for the future. These should show statistically representative statements about possible damage events that are characteristic for the rCF material. When these data are available, first coupled in-situ measurements can be carried out. By describing the AE signals for the rCF material more precisely, it is then possible to determine the load levels more precisely in the in-situ tests and to record the crack initiation and crack growth on the basis of the signals determined during the tests. These results can then be taken as a basis for automating the test procedure to reduce time and also reduce time-dependent effects in the material during the test series (creep, relaxation).

4 CONCLUSIONS

Despite the low fiber volume content, the UD sheets made of rCF staple fiber yarn with two different matrix systems show a good mechanical performance with 50 GPa stiffness and 550 MPa strength, which is, when extrapolated, similar to the already investigated sheets with a bio-resin matrix (cf. [6]). Nevertheless, it can be seen that the fiber-matrix adhesion is not optimal here either, although the PA6 shows slightly better adhesion, which is not reflected in a higher mechanical performance. The EP resin shows hardly any adhesion properties to the fiber, although the FTIR analysis of the existing sizing shows the better suitability of this matrix system. In order to achieve a general improvement of the fiber-matrix adhesion, further pretreatment of the fiber has to be considered.

The in-situ characterization of the damage behavior by means of X-ray microscopy in the transverse tensile test again provides the finding of a benign failure behavior. The crack propagation in the material is independent of areas with high fiber or matrix content but is mainly directed to the stress peaks in the specimen. If the specimen fails, the effect of fiber bridging also occurs here and leads to no structural

failure, only failure by load drop (no load is transferred to the specimen). The specimen remains intact and initially only fiber pullout takes place until the final breakup. Therefore, the inhomogeneity of the staple fiber yarn in processing leads to a positive behavior. This behavior can be exploited, for example, for crash-relevant components that are to exhibit structural integrity even after failure.

The approach of coupling AE and in-situ X-ray microscopy offers further advantages for characterizing the failure behavior in the future. Among other things, the new sample geometry can also detect the failure in the fiber direction. In addition, by recording the AE signal, possible damage events can be detected much more precisely and thus a much more targeted CT scan can be started. Thus, the three-dimensional representation of the damage process is much more precise and the simulative replication can also be realized more accurately.

REFERENCES

- [1] C. Goergen, *Quasiplastisches Verformungsverhalten von Organoblechen aus recycelten Kohlenstoff-Stapelfasergarnen*. Kaiserslautern: Institut für Verbundwerkstoffe GmbH, 2020.
- [2] C. Goergen, D. Schommer, M. Duhovic, and P. Mitschang, "Deep drawing of organic sheets made of hybrid recycled carbon and thermoplastic polyamide 6 staple fiber yarns," *Journal of Thermoplastic Composite Materials*, vol. 33, no. 6, pp. 754–778, 2020, doi: 10.1177/0892705718811407.
- [3] B. E. D. Meiners, Ed., *Recycling von Carbonfasern-Recycling und Rohstoffe - Band 7*. Neuruppin: TK-Verl., 2014. [Online]. Available: <http://www.vivis.de/fachbuecher/recycling-und-rohstoffe/184-rur7>
- [4] S. Pimenta and S. T. Pinho, "Recycling carbon fiber reinforced polymers for structural applications: technology review and market outlook," *Waste management (New York, N.Y.)*, vol. 31, no. 2, pp. 378–392, 2011, doi: 10.1016/j.wasman.2010.09.019.
- [5] H. Schürmann, *Konstruieren mit Faser-Kunststoff-Verbunden*, 2nd ed. Berlin, Heidelberg: Springer Berlin Heidelberg, 2007. [Online]. Available: <http://nbn-resolving.org/urn:nbn:de:bsz:31-epflicht-1576478>
- [6] C. Becker, N. Motsch-Eichmann, and J. Hausmann, "Analysis of the mechanical and fracture behavior of recycled carbon staple fiber yarn under static load," in *Proceedings of the 20th European Conference on Composite Materials - Composites Meet Sustainability (Vol 1-6)*, Lausanne, Switzerland, 2022, pp. 245–252.
- [7] J. Krummenacker and J. Hausmann, "Determination of Fatigue Damage Initiation in Short Fiber-Reinforced Thermoplastic through Acoustic Emission Analysis," *J. Compos. Sci.*, vol. 5, no. 8, p. 221, 2021, doi: 10.3390/jcs5080221.